Received: 9 September 2020 | Revised: 30 March 2021 | Accepted: 24 April 2021

IET Communications

DOI: 10.1049/cmu2.12238

The Institution of Engineering and Technology WILEY

ORIGINAL RESEARCH PAPER

Array antenna equipped UAV-BS for efficient low power WSN and its theoretical analysis

Hendrik Lumbantoruan | **Koichi Adachi**

Advanced Wireless and Communication Research Center, The University of Electro-Communications, Tokyo, Japan (Email: adachi@awcc.uec.ac.jp)

Correspondence
Hendrik Lumbantoruan, Advanced Wireless and Communication Research Center, The University of Electro-Communications, Chofu, Tokyo 182-8585, Japan.
Email: hendrik@awcc.uec.ac.jp

Funding information
Japan Society for the Promotion of Science, Grant/Award Number: JP18K04127

Abstract

In a wireless sensor network consisting of a large number of sensor nodes (SNs), an efficient communication scheme is crucial to boost data collection efficiency. Furthermore, SN is required to communicate by the low transmission power to prolong its battery life. However, SNs located at the edge of the communication area may fall into the outage as the signal-to-noise power ratio fails to surpass a certain threshold. Moreover, signal collision due to the interferers may deteriorate the packet delivery rate. An unmanned aerial vehicle-base station (UAV-BS) is an attractive solution to lower outage probability and enhance communication efficiency. Here, outage probability and capturing failure probability performance of a rotational angle division multiple access (RADMA), which is realized by UAV-BS with an array antenna, are analytically evaluated. The numerical performance evaluation is conducted to elucidate the performance improvement of RADMA under low power wide-area network setup. Numerical simulation results show that RADMA can suppress the packet loss ratio 77%, shorten the transmission time 25%, and reduce the required transmission energy 20%.

1 | INTRODUCTION

Wireless sensor network (WSN) with a large number of sensor nodes (SNs) has become one of the major research topics as it can be deployed to observe or monitor a particular area such temperature monitoring of a precision agriculture area [1–4]. Because of the difficulty of changing or recharging the battery once deployed [5], SNs are required to communicate with low power consumption to prolong its battery life. However, transmitting signals with low power may cause SNs to fall into an outage state as the signal-to-noise power ratio (SNR) fails to surpass a certain threshold at the receiver. Further, SNs located at the edge of the coverage area may be in an outage with a higher probability due to the long communication distance to the fusion center (FC). Therefore, low power transmission scheme is required to enable SNs to communicate in a low SNR range.

Recently, low power wide-area network (LPWAN) technologies are gaining a lot of interest due to its low power and large transmission coverage to support the Internet-of-things (IoT) with limited power supply. A long-range wide-area network (LoRaWAN) is one of the most pronounced LPWAN technologies and the most promising wide-area IoT technologies proposed by Semtech and further promoted by the LoRa Alliance [6]. In LoRaWAN, an adaptive data rate chirp spread-spectrum (CSS) modulation technology is adopted as a physical (PHY) layer technology to realize a flexible long-range communication with low power consumption and low cost. In CSS, different spreading factors (SFs) tune the chirp modulation rates. Lower SFs allow a high data rate but a short communication range, whereas higher SFs provide a long communication range at a low data rate. LoRaWAN is considered as a promising system to support WSN with a large number of low power SNs within a wide area.

In WSN, instead of centralized access control, the transmissions are carried out in an autonomously distributed manner by using random access schemes due to its simplicity [7]. Carrier sense multiple access/collision avoidance (CSMA/CA) is one of the random access schemes. In CSMA/CA, a signal collision happens when multiple SNs transmit simultaneously since each SN transmits in a distributed manner. The collided signal cannot be captured if the signal-to-interference power ratio (SIR) falls

below a certain threshold. The probability of the collided signal fails to be captured increases if the SIR decreases due to the interferers increment. Further, this capturing failure probability increases proportionally to the number of SNs in the WSN. Therefore, an efficient communication scheme is required to allow the SNs to communicate effectively without excessive collisions.

In recent years, using an unmanned aerial vehicle (UAV) as a base station (BS) has been considered a promising approach [8–10]. This is because unmanned aerial vehicle-base station (UAV-BS) can be deployed easily and dynamically at a low cost. UAV-BS provides several advantages. First, the probability of having line-of-sight (LoS) links to ground terminals is higher due to its high altitude [11]. Second, communication distance to each ground terminal can be shortened as UAV-BS can be dynamically placed closer to ground terminals or dense areas by leveraging its mobility [12]. Therefore, deploying UAV-BS as the FC of the WSN is considered as a promising approach to provide low power communication to SNs [13, 14].

1.1 | Related works

To ensure reliable communication to UAV, the authors of [15] investigated the optimum 2D placement of UAV for maximum reliability with total power loss and overall outage as the reliability measures. The altitude optimization of UAV to minimize the boundary outage probability of the coverage area was studied in [16]. To improve wireless coverage, the authors of [17] studied the optimal placement of multiple UAVs under different UAV altitude constraints and node densities to minimize the outage probability of node-to-UAV transmissions. The authors of [18] proposed an algorithm to enable a team of UAVs to cooperatively provide full coverage of an unknown field of interest while minimizing the overlapping sections among their field of views. These works show multiple UAVs are necessary to extend the coverage area. Meanwhile, more number of UAVs requires extra costs.

The authors of [19] considered deploying a UAV dynamically and formulated an optimal trajectory within a given time constraint to maximize the sum rate of ground nodes. A clustering based UAV positioning method to reduce the number of transmitting users and enhance network capacity was proposed in [20]. To avoid the excessive number of transmissions in a dense environment, the authors of [21] investigated the data collection scheme by clustering the nodes, constructing an optimized forwarding tree per cluster, and gathering the data from selected cluster-head nodes with minimized UAV trajectory distance. These works are limited to the UAV dynamic deployment method and vulnerable to the dense number of nodes. Further, the data collection scheme per cluster may lead to an excessive energy reduction of the selected cluster-head nodes. Meanwhile, WSNs in practical consist of a dense number of nodes with the same amount of energy.

In [22], we have proposed rotational angle division multiple access (RADMA), where UAV-BS is equipped with a uniform linear array antenna (ULA) to serve a subset of SNs at a time. In RADMA, a *virtual sector* is formed by exploiting the ULA's main lobe [23]. Since the signal from the outside of main lobe can be suppressed, the signals from the SNs within the virtual sector can be received with less interference. By this, the number of communicating SNs at a time can be limited. Furthermore, the signal transmitted from the SNs within the virtual sector can be enhanced by the high gain of ULA. The virtual sector is switched by horizontally rotating the UAV-BS with an appropriate time interval to cover the whole communication area.

In [22], the performance of RADMA has been investigated while adopting IEEE 802.11 as the wireless access protocol. Due to the limited coverage area, the system is not appropriate to monitor a wide agriculture area. Further, the performance of RADMA had been evaluated while limiting the number of SNs to 30. However, due to the large number of SNs connected within a WSN, it is required to validate if RADMA can work in a more practical situation.

In [24], outage probability (OP) of sensor nodes served by a ULA equipped UAV-BS has been conducted analytically. However, the location of the desired SN is assumed to be known by the UAV-BS. To gain more reliable results, it is required to deal with the locations of SNs as random variables. Further, the number of interfering signals may increase due to the increased number of SNs. Thus, it is necessary to analytically evaluate how the system deals with a certain amount of interferences.

1.2 | Contributions

In summary, the contributions of this manuscript are as follows.

1. Conducting analytical studies towards RADMA by evaluating its effectiveness from the viewpoint of OP and capturing failure probability to validate the accuracy of the numerical simulation results. The numerical results validated the derived equations are valid, and the proposed RADMA can suppress OP and capturing failure probability.
2. Investigating the performance of RADMA to serve a wider coverage area by applying LPWAN as the communication access protocol. The low received signal power of far-SNs due to the large path loss is the critical issue in this scenario. The simulation results elucidate that RADMA under the LPWAN scenario can tackle the low received signal power, hence far-SNs can transmit the data with a high transmission rate.
3. Investigating the performance of RADMA to serve a denser area to validate if RADMA can work in such practical situation. The increased number of SNs connected within a WSN is the critical issue in this scenario. The simulation results demonstrate how RADMA can suppress the number of lost packets, shorten transmission time, and reduce transmission energy in a various number of dense environment scenarios

The relation of related works and contributions are listed in Table 1.

The rest of the manuscript is organized as follows. In Section 2, the system and channel model are given. In Section 3, the proposed RADMA are described. In Section 4, the

outage probability and capturing effect analysis are conducted. In Section 5, the LoRaWAN network is described. Finally, some selected simulation results are provided in Section 6 in order to validate the newly derived analytical expression and the effectiveness of RADMA. Section 7 concludes the paper.

Notations: $\|\cdot\|$ is the norm, $\mathbb{E}[\cdot]$ is the expectation value, ${}_1F_1(\cdot,\cdot;\cdot)$ is the Kummer confluent hypergeometric function.

2 | SYSTEM AND CHANNEL MODEL

2.1 | System description

A UAV-BS is deployed as a mobile data collector, that is, FC, to gather information from a WSN consisting of K SNs. The number of SNs, K, is determined according to Poisson point process (PPP) of intensity λ_{SN} [/km^2]. The set of SNs is denoted by $\mathcal{K} = \{1, \dots, K\}$. The 2D location of SN $k \in \mathcal{K}$ is denoted by $\mathbf{w}_k = (x_k, y_k) \in \mathbb{R}^{2\times 1}$. All SNs are randomly and uniformly distributed within the coverage area with length of area side L_{AREA} [km]. Each SN generates a delay tolerant data packet and send it to the FC through CSMA/CA access protocol at the medium access control (MAC) layer. SN cannot sense other SN's signal if the signal power falls below a certain carrier sense (CS) threshold Γ_{CS}. All SNs transmit the signal with an omnidirectional antenna and with a fixed transmission power P_{T} [W].

This paper employs an unlicensed spectrum for the data collection from SNs. Consequently, the interferences from other systems (inter-system interference) that use the same unlicensed spectrum may exist. The inter-system interference will lead to an increased capturing failure probability. The performance degradation can be avoided by some mechanisms [25–27]. However, such mechanisms need to estimate or exchange information about parameters of the other systems such as transmission time and transmission interval. Our main objective is to tackle the interference problem among SNs in the same system and theoretically analyse its performance. Since the proposed system is not exclusive with the other mechanisms to deal with inter-system interference, considering the interferences from other systems will remain as our future work. Thus, this paper assumes that inter-system interference does not exist.

2.2 | Channel model

The channel for each communication link between UAV-BS and SN k is modeled with path loss and shadowing loss. In particular, we consider a free-space path loss, which is given by [28]

$$L_k(d_k) = \left(\frac{4\pi f_{\mathrm{c}} d_k}{c}\right)^2, \tag{1}$$

where f_{c} is the carrier frequency [Hz] and c is the speed of light [m/s]. The distance between the UAV-BS and SN k, d_k [m], can be calculated as

$$d_k = \sqrt{\|\mathbf{w}_{\mathrm{UAV}} - \mathbf{w}_k\|^2 + H_{\mathrm{UAV}}^2}, \tag{2}$$

where $\mathbf{w}_{\mathrm{UAV}} = (x_{\mathrm{UAV}}, y_{\mathrm{UAV}}) \in \mathbb{R}^{2\times 1}$ and H_{UAV} are the 2D location and the altitude of the UAV-BS, respectively. Since the distance between UAV-BS and each SN is much larger than the terrain height differences between SNs, it is reasonable to assume that the ground is flat.

The log-normally distributed shadowing loss [dB] is given by [30]

$$\psi_{k,\mathrm{dB}} = P_{\mathrm{LoS},k}\psi_{\mathrm{LoS},k} + P_{\mathrm{NLoS},k}\psi_{\mathrm{NLoS},k}, \tag{3}$$

where $\psi_{\mathrm{LoS},k}$ and $\psi_{\mathrm{NLoS},k}$ are shadow fading coefficient with log-normal distribution for LoS and NLoS link, respectively [30].

$$\begin{cases} \sigma_{\mathrm{LoS},k} = k_1 \exp(-k_2\theta_k) \\ \sigma_{\mathrm{NLoS},k} = g_1 \exp(-g_2\theta_k) \end{cases}, \tag{4}$$

where $(\mu_{\mathrm{LoS},k}, \sigma^2_{\mathrm{LoS},k})$ and $(\mu_{\mathrm{NLoS},k}, \sigma^2_{\mathrm{NLoS},k})$ are the mean and the variance of the shadow fading for LoS and NLoS link, respectively. k_1, k_2, g_1, g_2 are constant values which depend on environment. $\theta_k = \sin^{-1}(H_{\mathrm{UAV}}/d_k)$ is the elevation angle between UAV-BS and SN k. Finally, the LoS probability is given by [30]

$$P_{\mathrm{LoS},k} = \alpha\left(\frac{180}{\pi}\theta_k - 15\right)^{\beta}, \tag{5}$$

where α and β are constant values which depend on environment. Here, $P_{\mathrm{NLoS},k} = 1 - P_{\mathrm{LoS},k}$. (5) indicates that as H_{UAV} becomes higher, the LoS probability becomes larger.

The received signal power from SN k at UAV-BS can be expressed as

$$\Omega_k = \frac{P_{\mathrm{T}}}{B}\frac{G_{\mathrm{T}}G_{\mathrm{R}}}{L_k\psi_k}, \tag{6}$$

where G_{T} and G_{R} are the antenna gain of SN and UAV-BS [dB], respectively. B is the bandwidth [kHz] and $\psi_k = 10^{\psi_{k,\mathrm{dB}}/10}$.

Without loss of generality, SN $k = 0$ is considered as the desired SN. The received signal of the desired SN at the UAV-BS can be expressed as

$$r = \sqrt{\Omega_0}h_0 s_0 + \sum_{k=1}^{K}\sqrt{\Omega_k}h_k s_k + w, \tag{7}$$

where h_k denotes the fading coefficient between UAV-BS and SN k which follows non-centered chi-squared distribution and $w \sim \mathcal{CN}(0, \sigma^2)$ is the additive white Gaussian noise (AWGN) with 0 mean and variance σ^2.

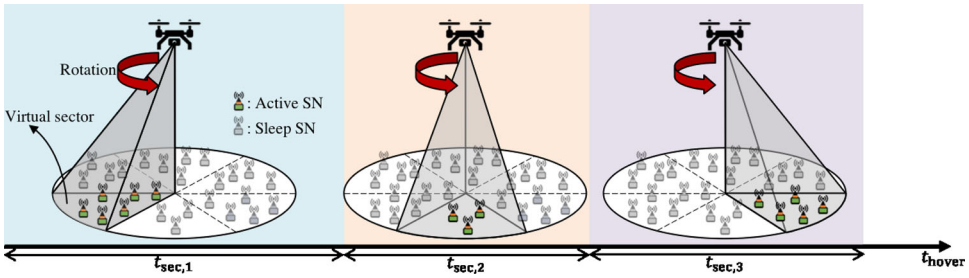

FIGURE 1 Concept of RADMA

3 | PROPOSED METHOD: RADMA

RADMA is a communication access method that splits the coverage area into partially overlapping *virtual sectors*, as shown in Figure 1. In this method, the UAV-BS is equipped with a ULA. The main lobe of ULA beam is exploited to form the virtual sector.

At first, all SNs are in sleep mode while waiting to be served by the UAV-BS. After receiving the beacon signal from the UAV-BS, only the SNs within the virtual sector can switch from sleep mode to active mode due to the channel condition. Thus, the number of communicating SNs can be limited to avoid excessive signal collisions. Further, the high gain of ULA can be exploited to enhance the received signal power of SNs. Thus, the outage probability can be lowered, and a higher transmission rate can be assigned due to the enhanced received signal power.

3.1 | Rotation and allocation time

To provide communication opportunities to all SNs, virtual sectors are created by horizontally rotating the UAV-BS to cover all coverage area, as shown in Figure 1. After serving the SNs within a certain virtual sector, the UAV-BS will be rotated with a specific rotational angle. If the UAV-BS is rotated with rotational angle $\theta_{\mathrm{RT}} \in \{0, 2\pi\}$, number of sectors J is given by

$$J = \frac{2\pi}{\theta_{\mathrm{RT}}}. \tag{8}$$

The UAV-BS will serve a certain virtual sector within an allocated time. The allocated time will be adjusted to the number of SNs within the sector. A longer time will be allocated to the sector with a larger number of SNs, as shown in Figure 1. The allocated time to virtual sector j, that is, *sector time* $t_{\mathrm{sec},j}$, is given by

$$t_{\mathrm{sec},j} = \frac{K_j}{K}(t_{\mathrm{hover}} - t_{\mathrm{rotation}}), \tag{9}$$

where K_j is the number of SNs within virtual sector $j = \{1, \ldots, J\}$, t_{hover} and t_{rotation} are the hovering time and the rotation time of UAV-BS that is calculated as $t_{\mathrm{rotation}} = \frac{360^\circ}{v_{\mathrm{ang}}}$ with v_{ang} being the angular speed of UAV, respectively. The performance of RADMA with various number of sector J and sector time $t_{\mathrm{sec},j}$ allocation method had been discussed in [22].

3.2 | ULA gain and tilt angle

The gain of ULA towards SN k with direction-of-arrival (DoA) ϕ_k is given by [28]

$$G_{\mathrm{R},k} = \left| \sum_{m=0}^{M-1} g(\theta_k, \phi_k) \mathrm{e}^{-j2\pi m \Delta \sin\theta_k \cos\phi_k} \right|^2, \tag{10}$$

where M and Δ are the number of antenna elements and the antenna element spacing normalized by the carrier wavelength, respectively. $g(\theta_k, \phi_k)$ is the directivity of the antenna element towards horizontal angle ϕ_k and elevation angle θ_k. In this manuscript, a half-wave dipole antenna is used for each antenna element, and hence directivity $g(\theta_k, \phi_k)$ is given by [28]:

$$g(\theta_k, \phi_k) = \sqrt{1.64} \cos\left(\frac{\pi}{2} \cos\theta_k\right) / \sin\theta_k. \tag{11}$$

In this manuscript, tilt angle θ_{tilt} is determined to adjust the direction of the main beam as shown in the following equation:

$$\theta_{\mathrm{tilt}} = \frac{\pi}{2} - \tan^{-1}\left(\frac{r/2}{H_{\mathrm{UAV}}}\right), \tag{12}$$

where the numerator in arctangent is determined into $r/2$ so the main beam can be set to face the center of the coverage radius r. The purposes are to maximize the use of the antenna's beam and to fairly serve the near-SNs and far-SNs. Substituting (12) into (10) gives

$$G_{\mathrm{R},k} = \left| \sum_{n=0}^{M-1} g(\theta_k, \phi_k) \mathrm{e}^{-j2\pi n \Delta \sin(\theta_k + \theta_{\mathrm{tilt}}) \cos\phi_k} \right|^2, \tag{13}$$

where

$$g(\theta_k, \phi_k) = \sqrt{1.64} \frac{\cos\left(\frac{\pi}{2} \cos(\theta_k + \theta_{\mathrm{tilt}})\right)}{\sin(\theta_k + \theta_{\mathrm{tilt}})}. \tag{14}$$

As distance d_k between the UAV-BS and SN k is much larger than antenna element spacing Δ, it is reasonable to assume that there is only one strong link between the UAV-BS and SN [31].

4 | OUTAGE PROBABILITY AND CAPTURING EFFECT ANALYSIS

OP is defined as the probability that achievable SNR γ_0 of the desired SN falls below a certain SNR threshold γ_{th}. Thus, it is necessary to derive the SNR expression before analysing the OP. Similar to OP, the capturing failure probability is defined as the probability that the SIR β_0 of the desired SN falls below a certain SIR threshold β_{th}. Thus, deriving the SIR expression is necessary before analysing the capturing failure probability.

4.1 | Outage probability closed-form expression derivation

The closed-form expression of the OP is derived for a system experiencing Rician fading. This work has been pursued with a similar approach in [24], which derives a closed-form expression of the probability density function (PDF) and cumulative distribution function (CDF) of independent random variables (RVs). The required material is only an infinite power series expansion of the CDF of the desired SN's signal power.

The instantaneous SNR of desired SN $k = 0$, γ_0, is expressed as

$$\gamma_0 = \frac{\Omega_0 |h_0|^2}{\sigma^2}. \tag{15}$$

To derive the average achievable SNR, the average received signal power $\overline{\Omega_k}$ of SN k will be derived based on the communication protocol. To simplify, the shadowing loss is excluded from the received signal power equation.

1. **Conventional method**
   Conventional method is the method where the UAV-BS is equipped with an omni-directional antenna to serve the communication area at once. Thus, the average received signal power $\overline{\Omega_k}$ of SN k can be derived as

$$\overline{\Omega_k} = \frac{P_{\text{T}}}{B} \frac{G_{\text{T}} G_{\text{R}}}{\overline{L_k}}, \tag{16}$$

   where $\overline{L_k}$ is the mean value of path loss L_k of SN k.
2. **RADMA**
   The average received signal power $\overline{\Omega_k}$ of SN k can be derived as

$$\overline{\Omega_k} = \frac{P_{\text{T}}}{B} \frac{G_{\text{T}} \overline{G_{\text{R},k}}}{\overline{L_k}}, \tag{17}$$

   where $\overline{G_{\text{R},k}}$ is the mean value of ULA gain $G_{\text{R},k}$ towards SN k within the virtual sector.

$\overline{L_k}$ can be expressed by applying the mean value theorem [32] as

$$\overline{L_k} = \frac{1}{\sqrt{R^2 + H_{\text{UAV}}^2} - H_{\text{UAV}}} \int_{H_{\text{UAV}}}^{\sqrt{R^2 + H_{\text{UAV}}^2}} L_k(d_k) \delta d, \tag{18}$$

where $\sqrt{R^2 + H_{\text{UAV}}^2}$ is the farthest distance of SN located at the edge of the coverage area to UAV-BS while H_{UAV} is the shortest distance of SN to UAV-BS when located under the UAV-BS.

Similar to (18), $\overline{G_{\text{R},k}}$ can be expressed as

$$\overline{G_{\text{R},k}} = \frac{1}{(W_{\text{U}} - W_{\text{L}}) \tan^{-1} \frac{R}{H_{\text{UAV}}}} \times \int_0^{\tan^{-1} \frac{R}{H_{\text{UAV}}}} \int_{W_{\text{L}}}^{W_{\text{U}}} G_{\text{R},k} \delta\phi \delta\theta, \tag{19}$$

where W_{L} and W_{U} are the minimum angle and maximum angle of the ULA beam coverage range, respectively, and $\tan^{-1}(\frac{R}{H_{\text{UAV}}})$ is the available range of θ.

Then, achievable SNR γ_0 can be expressed as

$$\gamma_0 = \frac{\overline{\Omega_0} |h_0|^2}{\sigma^2} = \frac{S_0}{\sigma^2}. \tag{20}$$

The OP of the desired SN is defined as the probability that achievable SNR γ_0 falls below a certain threshold γ_{th}, that is

$$P_{\text{out}}(\gamma_{\text{th}}) = P(\gamma_0 < \gamma_{\text{th}}). \tag{21}$$

Lemma 1: Outage probability, $P_{\text{out}}(\gamma_{\text{th}})$, is given by

$$P_{\text{out}}(\gamma_{\text{th}}) = \sum_{n=0}^{\infty} \frac{e^{-K_0} L_n^{(0)}(K_0)(1 + K_0)^{n+1}}{(1 + n)! \overline{\Omega_0}^{n+1}} (\gamma_{\text{th}} \sigma^2)^{n+1}. \tag{22}$$

Proof. The proof is given in Appendix A.

4.2 | Capturing effect analysis

Similar to the closed-form expression of the OP, the capturing probability is derived for a system experiencing Rician fading. Capturing probability is derived while assuming number of interfering SNs I to investigate how the system dealing to interferences. The required materials are (1) an infinite power series expansion of the CDF the desired SN's signal power and (2) expressions for the moments of the co-channel power from interferers. Instantaneous SIR β_0 of the desired SN, $k = 0$, is

expressed as

$$\beta_0 = \frac{\Omega_0 |h_0|^2}{\sum_{i=1}^{I} \Omega_i |h_i|^2}. \tag{23}$$

Similar to (20), by substituting average received signal power $\overline{\Omega_k}$ into (23), achievable SIR β_0 of the desired SN can be expressed as

$$\beta_0 = \frac{\overline{\Omega_0} |h_0|^2}{\sum_{i=1}^{I} \overline{\Omega_i} |h_i|^2} = \frac{S_0}{\sum_{i=1}^{I} S_i}. \tag{24}$$

The signal from desired SN is not able to be successfully received at FC if its SIR β_0 falls bellow a certain SIR threshold β_{th}. Thus, capturing failure probability P_{fail} is given by

$$P_{\text{fail}}(\beta_{\text{th}}) = P(\beta_0 < \beta_{\text{th}}). \tag{25}$$

Lemma 2: Capturing failure probability $P_{\text{fail}}(\beta_{\text{th}})$ is given by

$$P_{\text{fail}}(\beta_{\text{th}}) = \sum_{n=0}^{\infty} \frac{e^{-K_0} L_n^{(0)}(K_0)(1+K_0)^{n+1}}{(1+n)!\overline{\Omega_0}^{n+1}} \beta_{\text{th}}^{n+1} \times \sum_{i_1+\cdots+i_I=n+1} \binom{n+1}{i_1, \ldots, i_K} \prod_{j=1}^{I} \mathbb{E}[S_i^{i_j}], \tag{26}$$

where $\mathbb{E}[S_i^{i_j}]$ is the cross-moment of the RVs $(S_1, S_2, \ldots, S_I)$ and $\binom{n}{i_1,\ldots,i_I}$ is the multinomial coefficient which is given by

$$\binom{n}{i_1, \ldots, i_I} = \frac{n!}{i_1! \ldots i_I!}. \tag{27}$$

Proof: The proof is given in Appendix B.

4.3 | Convergence radius

In order to guarantee the validity of the derived capturing failure probability in (26), it is necessary to investigate the convergence of the power series expansion by providing sufficient conditions that ensure its convergence.

Similar to the previous section, it is considered that both the desired and the interfering signal(s) experience the Rician fading environment. Then, received power S_0 of the desired SN is a non-centered chi-squared distribution with a rice factor K_0 and an average power $\overline{\Omega_0}$. Similarly, received power $\{S_i\}_{i=1}^{I}$ of the interfering SN(s) follow non-centered chi-squared distributions with rice factors $\{K_i\}_{i=1}^{I}$ and average powers $\{\overline{\Omega_i}\}_{i=1}^{I}$.

Theorem 1: Let S_0 be a non-centered chi-squared distribution with parameters K_0 and $\overline{\Omega_0}$, and $S_1, S_2, \ldots, S_I$ be correlated RVs following non-centered chi-squared distributions with parameters $\{K_i\}_{i=1}^{I}$ and $\{\overline{\Omega_i}\}_{i=1}^{I}$. Then, the convergence radius γ_{th} satisfies:

$$\beta_{\text{th}} < \frac{\overline{\Omega_0}(1+K_i)}{(1+K_0)\overline{\Omega_i} I}, \forall i. \tag{28}$$

Proof: The proof is given in Appendix C.

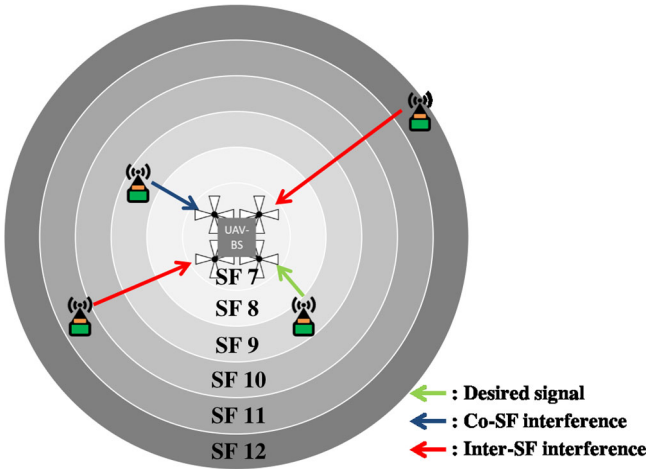

FIGURE 2 LoRaWAN system setup: Distance based SF allocation

5 | LoRaWAN NETWORK

In LoRaWAN, the CSS modulation technique is adopted as the PHY layer technology. Each chirp or symbol will be assigned to transmit a constant/fixed number of bits. The amount of bits per each symbol is called the spreading factor (SF) which varies from 7 to 12. As the SF increases, the receiver's sensitivity increases and the communication range becomes wider, as shown in Figure 2. The transmission rate, $R_{\text{T}}(f)$, of SF $f \in \{7, 8, \ldots, 12\}$ is given by

$$R_{\text{T}}(f) = \frac{f \times R_{\text{C}}}{T_m}, \tag{29}$$

where $T_m = \frac{2^f}{B}$ is the symbol duration and R_{C} is the coding rate. The required SNR threshold $\gamma_{\text{th}}(f)$ for each SF to achieve the bit error rate (BER) with value of 10^{-5} has been calculated in [33]. Accordingly, transmission rate $R_{\text{T}}(f)$ and required SNR threshold $\gamma_{\text{th}}(f)$ for each SF are shown in Table 2.

Recent results on LoRaWAN in [35–37] have shown through real experiments and numerical analysis that a signal transmitted by a LoRaWAN device to the gateway may suffer two kinds of disruption. This disruption can be either caused by co-SF interferences (i.e. interferences transmitted from the same SF) or cross-SF interferences (i.e. interferences transmitted from different SFs). Thus, to be correctly decoded, it is required to consider the SIR threshold based on the origin SF of the interfering signal.

TABLE 1 Summary of the contributions

Related works	Contributions
[15] Optimum 2D placement of UAV has been investigated to lower overall outage	Proposing RADMA to serves an amount number of nodes within a wide area by using only a single UAV on a non-dynamic deployment
[16] Altitude optimization of UAV has been investigated to minimize the boundary outage probability	
[17] Optimal placement of multiple UAVs has been studied under different UAV altitude constraints and node densities to minimize the outage probability	
[18] An algorithm has been proposed to enable a team of UAVs to provide full coverage of an unknown field of interest cooperatively	
[19] Optimal trajectory has been formulated to maximize sum rate	Exploiting virtual sector to limit the number of transmitting nodes, and to enhance the received signal power of nodes by the high gain of ULA to use high transmission rate
[20] Clustering based UAV positioning method has been proposed to enhance network capacity	
[21] Clustering based data collection scheme has been investigated to enable UAV collect the data effectively within minimized trajectory	
[22] RADMA is originally proposed	Conducting analytical studies towards RADMA to evaluate its effectiveness from the viewpoint of the outage probability and capturing failure probability
[24] Outage probability of sensor nodes served by a ULA equipped UAV-BS has been conducted analytically while assuming the location of node is known and no interference exist	
[22] The performance of RADMA has been investigated within a limited coverage area and limited number of nodes by adopting IEEE 802.11 as the wireless access protocol	Investigating the performance of RADMA under the LPWAN scenario to expand the coverage area and evaluating it in a denser environment scenario

TABLE 2 Transmission rate, SNR and SIR threshold of each SF$B = 125$ [kHz], $R_C = 4/5$)

SF	Rate [kbps]	SNR threshold [dB]	SIR threshold [dB]
7	5.469	−7.5	−11
8	3.125	−10	−13
9	1.758	−12.5	−16
10	0.977	−15	−19
11	0.537	−17.5	−22
12	0.293	−20	−24

In [35], a co-SF SIR threshold of 6 [dB] has been assumed based on average measurements of communication between two LoRaWAN devices. Thus, when co-SF interferences exist, a certain signal can be successfully decoded if its SIR surpasses 6 [dB].

In [36], the inter-SF SIR thresholds of a certain signal to be successfully decoded are summarized. These SIR thresholds are defined to achieve a BER of approximately 1%. These thresholds for each SF depend on the interfering signal's origin SF. The threshold is bigger if the interfering signal's origin SF is the desired signal's neighbor SF. Accordingly, this threshold is considered as the worst case for each SF. As multiple signals transmitted from different SFs may collide simultaneously, it is reasonable to set the worst thresholds for each SF as the inter-SF SIR threshold. The inter-SF SIR thresholds of a certain signal to be successfully decoded is shown in Table 2.

The transmitted signal can be received successfully at gateway if one or more of these conditions are satisfied:

1. **Reception condition**
   The received SNR of a certain LoRaWAN device at a given SF f surpasses the certain SF threshold (see Table 2).
2. **Co-SF capture threshold**
   When the desired and interfering signals are transmitted with the same SF, the signal from the desired device can be correctly captured if the SIR surpasses the co-SF SIR threshold.
3. **Inter-SF capture threshold**
   When the desired and interfering signals are transmitted with the different SFs, the signal from the desired device can be correctly captured if the SIR surpasses the inter-SF SIR threshold.

6 | NUMERICAL RESULTS

In this section, the numerical results are provided. These results are obtained by executing computer simulation by constructing the system model into C language and MATLAB. The hovering altitude of UAV-BS, H_{UAV} [km], is set varying up to 0.12 [km] since it is the maximum permitted altitude for UAV-BS in many jurisdictions [38]. Length of area side L_{AREA} [km] and intensity of SNs λ_{SN} [/km^2] are set as parameters to validate the performance of RADMA on various L_{AREA} and λ_{SN}. Number of antenna elements N of the ULA at UAV-BS is set to 3, and normalized antenna elements spacing Δ is set to 0.5[28]. Transmit power P_{T} and antenna gain G_{T} at SN are set to 13 [dBm] and 0 [dBi], respectively [2]. The carrier frequency is set to $f_c = 923$ [MHz] and the bandwidth is $B = 125$ [kHz] [34]. Other parameters are listed in Table 3.

This paper assumes that each SN has only one packet to transmit during each simulation. The packet size is set as the

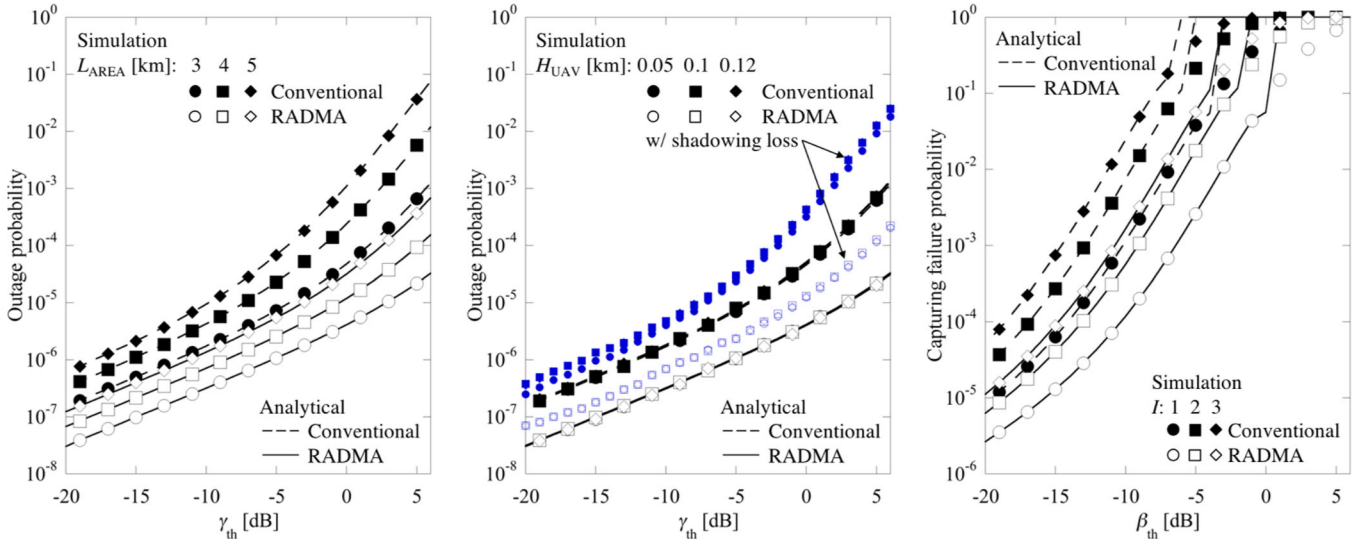

FIGURE 3 (a, b) $P_{out}(\gamma_{th})$ versus γ_{th} and (c) $P_{fail}(\beta_{th})$ versus β_{th}

largest packet size that can be transmitted using SF12 within the dwell time. The dwell time is defined by the maximum time to transmit 1 packet by a LoRaWAN device and is standardized to 400 [ms] [34]. The transmission rate of SN in SF12 is 293 [bps] as shown in Table 2. Thus, the largest packet size that can be transmitted using SF12 within the standardized dwell time is about 100 [bit]. As each SN will transmit only once without repetition, the duty cycle is not considered.

6.1 | Outage probability and capture effect analysis

In Figure 3a, the analytical and the simulated values of OP $P_{out}(\gamma_{th})$ are plotted as a function of γ_{th} for various length of area side L_{AREA} while UAV-BS altitude H_{UAV} is fixed at 0.1 [km]. Figure 3a shows that the OP increases as length of area side L_{AREA} becomes bigger. This is because the SNs deployed at the edge of the coverage area experience large path loss due to the long transmission link distance. Thus, the achievable SNR fails to surpass the required SNR for communication. However, RADMA can suppress OP compared to the conventional method for any length of area side L_{AREA}. This is because the achievable SNR of SNs can be enhanced by exploiting the high gain of ULA.

Table 4 shows the relative errors between the analytical and the simulated values of OP $P_{out}(\gamma_{th})$ for various SNR threshold γ_{th} and length of area side L_{AREA}. The Table clearly shows that the relative errors between the analytical and the simulated values of OP $P_{out}(\gamma_{th})$ are far away below 1% for both RADMA and conventional method. This clearly indicates the validity of the derived closed-form OP expression.

In Figure 3b, the analytical and the simulated values of OP $P_{out}(\gamma_{th})$ are also plotted as a function of γ_{th} for various UAV-BS altitude H_{UAV} while length of area side L_{AREA} is set to 3 [km]. Similar to Figure 3a, this figure also clearly shows that the analytical and simulated results match perfectly which indicates the validity of the derived closed-form OP expression. UAV-BS altitude H_{UAV} does not impact the OP. This is because length of area side L_{AREA} is much bigger than UAV-BS altitude H_{UAV}. Thus the variation of UAV-BS altitude H_{UAV} does not give a significant impact to the achievable SNR. However when considering the shadowing loss, the OP differs as UAV-BS altitude H_{UAV} increases. This is because the achievable SNR varies caused by the shadowing loss.

TABLE 3 Computer simulation parameters

Parameters	Values
Length of area side	$L_{AREA} = 3, 4, 5$ [km]
Intensity of SNs	$\lambda_{SN} = 20, 40, 60$ [/km^2]
UAV-BS altitude	$H_{UAV} = 0.05, 0.1, 0.12$ [km]
UAV-BS antenna elements	$N = 3$
UAV-BS angular speed	$v_{ang} = 250$ [°/s] [29]
Normalized antenna spacing	$\Delta = 0.5$
Rotation angle	$\theta_{RT} = \frac{2\pi}{6}$ [radian]
SN's height	0.1 [m]
SN's antenna gain	$G_T = 0$ [dBi]
SN's transmit power	$P_T = 13$ [dBm]
SN's data size	$S = 100$ [bits]
Carrier frequency	$f_c = 923$ [MHz]
Bandwidth	$B = 125$ [kHz]
CS threshold	$\Gamma_{CS} = -97$ [dBm][28]
Noise variance	$\sigma^2 = -174$ [dBm/Hz]
Noise figure	10 [dB]
Order of truncation	$K_{tr} = 10$
Rice factor	$K_0 = 10$, $K_i = 10$
k_1, k_2, g_1, g_2	11.53, 0.06, 26.53, 0.03 [30]
μ_{LoS}, μ_{NLoS}	0.0, 18 [dB] [30]
α, β	0.77, 0.05 [30]

TABLE 4 Relative errors between the simulated and analytical values of $P_{\text{out}}(\gamma_{\text{th}})$ (various L_{AREA} [km])

γ_{th}	RADMA			Conventional		
[dB]	3	4	5	3	4	5
−20	0.02%	0.19%	0.02%	0.20%	0.06%	0.10%
−19	0.02%	0.38%	0.19%	0.01%	0.08%	0.19%
−18	0.05%	0.01%	0.06%	0.01%	0.05%	0.08%
−17	0.02%	0.10%	0.05%	0.06%	0.16%	0.07%
−16	0.34%	0.21%	0.05%	0.01%	0.36%	0.21%
−15	0.34%	0.20%	0.05%	0.06%	0.14%	0.06%
−14	0.05%	0.06%	0.02%	0.38%	0.23%	0.01%
−13	0.09%	0.05%	0.01%	0.02%	0.02%	0.04%
−12	0.15%	0.01%	0.26%	0.06%	0.13%	0.25%
−11	0.04%	0.07%	0.15%	0.18%	0.00%	0.62%
−10	0.09%	0.07%	0.04%	0.18%	0.06%	0.30%
−9	0.06%	0.38%	0.05%	0.02%	0.14%	0.82%
−8	0.03%	0.27%	0.20%	0.74%	0.50%	0.55%
−7	0.28%	0.74%	0.11%	0.48%	0.03%	0.01%
−6	0.11%	0.60%	0.38%	0.58%	0.75%	0.59%
−5	0.18%	0.39%	0.30%	0.78%	0.57%	0.31%
−4	0.06%	0.67%	0.45%	0.20%	0.96%	0.18%
−3	0.08%	0.27%	0.02%	0.96%	0.19%	0.19%
−2	0.14%	0.19%	0.48%	0.37%	0.43%	0.09%
−1	0.35%	0.07%	0.55%	0.71%	0.63%	0.02%
0	0.23%	0.41%	0.17%	0.94%	0.05%	0.35%
1	0.47%	0.49%	0.31%	0.27%	0.13%	0.04%
2	0.10%	0.01%	0.30%	0.35%	0.05%	0.05%
3	0.46%	0.88%	0.02%	0.33%	0.14%	0.16%
4	0.37%	0.88%	0.48%	0.01%	0.01%	0.88%
5	0.25%	0.59%	0.00%	0.16%	0.07%	0.76%
6	0.28%	0.15%	0.14%	0.11%	0.36%	0.22%

In Figure 3c, the analytical and the simulated values of capturing failure probability $P_{\text{fail}}(\beta_{\text{th}})$ are plotted as a function of SIR threshold β_{th} for various number of interferers I. Length of area side L_{AREA} and UAV-BS altitude H_{UAV} are set to 3 [km] and 0.1 [km], respectively. From these results, it can be concluded that the derived closed-form expression β_{th} is valid as both analytical and simulated values perfectly match. Figure 3c also shows that derived $P_{\text{fail}}(\beta_{\text{th}})$ starts to diverge and show different results with the simulated results as β_{th} increases and becomes closer to the higher bound of β_{th}. This indicates that the derived convergence radius is valid.

Figure 3c also shows that RADMA can suppress $P_{\text{fail}}(\beta_{\text{th}})$ compared to the conventional method for any number of interfering SN I. This is because, in RADMA, the signal from the desired SN can be prioritized by the ULA beam direction, which leads to higher received signal power Ω_0 of the desired SN at UAV-BS. In the other side, received signal power Ω_i of the interfering SNs can be suppressed due to the poor channel condition outside of the ULA beam. Thus, the achievable SIR can be enhanced and surpass a certain threshold. This means the collided signals are still possible to be captured successfully.

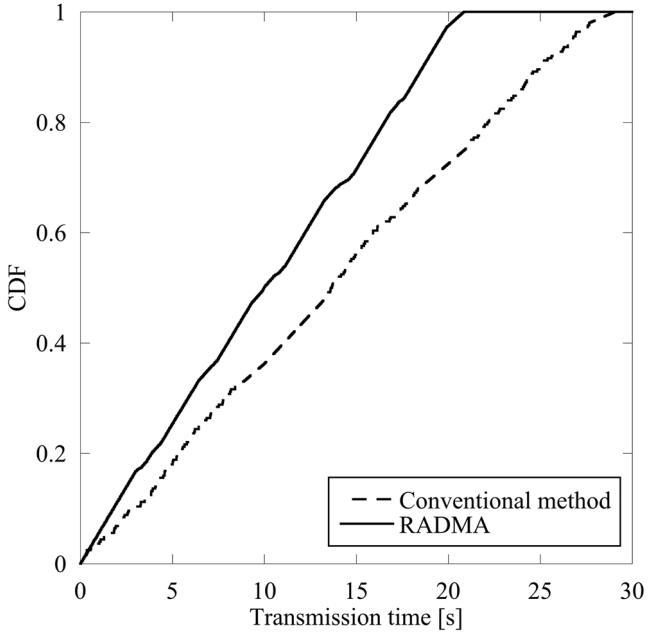

FIGURE 4 CDF of transmission time (L_{AREA}=5 [km], λ_{SN}=20 [/km^2])

6.2 | RADMA performance towards area size

In this section, the CDF of the required transmission time is investigated and the performance of RADMA is evaluated with various length of area side L_{AREA}. Intensity of SNs λ_{SN} and UAV-BS altitude H_{UAV} are fixed to 20 [/km^2] and 0.1 [km], respectively. First, the packet loss ratio (PLR) is evaluated. PLR is defined as the number of lost packets divided by the total number of packets. The lost packet is the packet that fails to fulfill the successful reception conditions described in Section 2. Second, the average required time for one packet transmission is evaluated. Finally, the average transmission energy to complete the packet transmission, defined by the multiplication of transmission time and transmission power, is evaluated.

Figure shows the CDF of the required transmission time to transmit the data packet. Even considering the stand by time to be served, RADMA can suppress the accumulation time to complete the transmission. This is because RADMA enables SNs to transmit at a higher transmission rate due to the enhanced received signal power by ULA's high gain. Further, SNs can effectively execute the transmission due to the limited number of SNs within the virtual sector.

Figure 5a shows the PLR increases as the length of area side L_{AREA} becomes bigger. This is because the excessive signal collisions frequently happened as the probability of carrier sense failure between SNs increases due to large path loss caused by the long distance between SNs. Further, the number

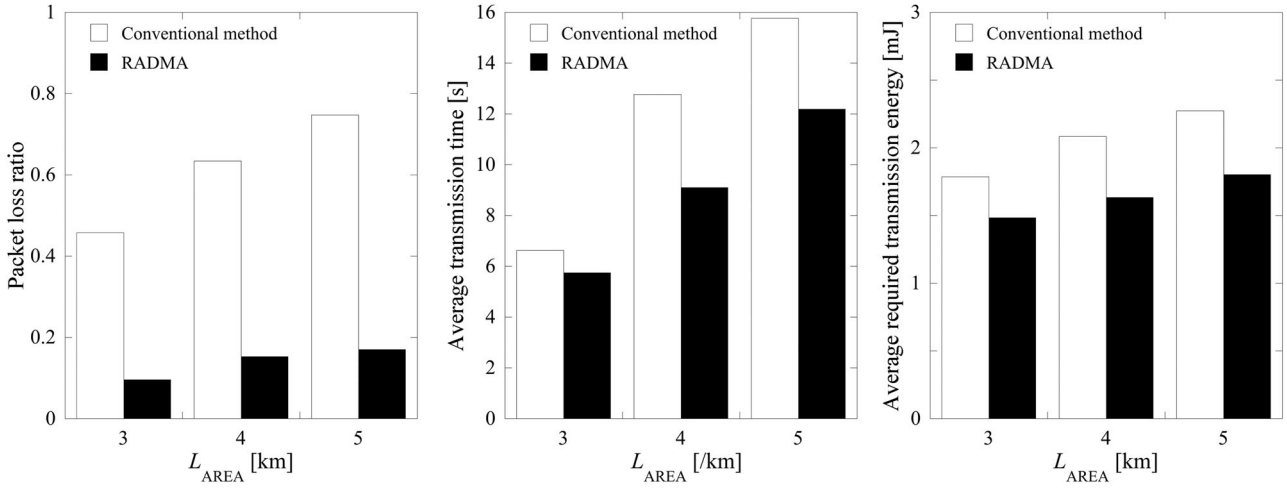

FIGURE 5 Performance comparison of RADMA and conventional method (various length of area side L_{AREA})

of SNs increases as the area becomes wider. Thus, the probability that multiple SNs transmit simultaneously increases. However, the PLR can be suppressed by RADMA up to 77% compared to the conventional method when considering area side $L_{\mathrm{AREA}} = 5$ [km]. This happens by exploiting the benefits of ULA beam: limiting the number of SNs simultaneously transmitting a packet, alleviating the hidden terminal problem, and enhancing the received signal power of the desired SN while suppressing the received signal power of interfering SNs. Therefore, RADMA can guarantee a high packet delivery ratio even in a wider area.

Figure shows the average transmission time increases as the length of area side L_{AREA} becomes bigger. This is because the applicable transmission rate decreases due to the lower received signal power caused by larger path loss. However, the transmission time can be shortened by RADMA up to 25% compared to the conventional method when considering area side $L_{\mathrm{AREA}} = 5$ [km] even considering the standby time to be served. This is because higher transmission rate is applicable due to the enhanced received signal power.

Figure 5c shows the average transmission energy to complete the data transmission, which has a similar pattern to the average transmission time shown in Figure 5b. From Figure 5c, it can be seen that the average required transmission energy can be suppressed up to 20% by RADMA compared to the conventional method when considering area side $L_{\mathrm{AREA}} = 5$ [km]. The reason is that RADMA can shorten the transmission time due to the high transmission rate. Therefore, the required energy to complete the data transmission can be reduced accordingly.

6.3 | RADMA performance towards intensity of SNs

Here, the performance of RADMA is evaluated for the various intensity of SNs λ_{SN}. Length of area side L_{AREA} and UAV-BS altitude H_{UAV} are set to 3 [km] and 0.1 [km], respectively.

Figure 6a shows the PLR increases as the intensity of SNs λ_{SN} increases. This is because the probability of multiple SNs transmit simultaneously increases when the environment becomes denser. However, the PLR can be suppressed by RADMA due to the reasons described in the previous section. Hence, RADMA can guarantee a high packet delivery ratio even in a dense SNs environment.

Figure 6b shows the average transmission time increases as the intensity of SNs λ_{SN} increases. This is because the standby time of SNs increases as the environment becomes denser. Further, the SNs located at the edge transmit the signal with a low transmission rate due to the low received signal power. However, the transmission time can be shortened by RADMA even considering the standby time to be served. This is because higher transmission rate is applicable due to the enhanced received signal power.

Figure 6c shows the average transmission energy of each SN to complete the data transmission. From Figure 6c, it can be seen that the average transmission energy can be suppressed by applying RADMA compared to the conventional method. However, the average required transmission energy is insensitive to λ_{SN}. The reason can be explained as follows. All the SNs within the serving sector can be fairly served by facing the main beam to the center of the coverage radius. Since the near-SNs and far-SNs can experience similar transmission link quality, the average required transmission energy will remain low even with denser SNs.

7 | CONCLUSION

In a WSN with a large number of SNs, a low power consumption and efficient communication scheme is crucial to prolong the network lifetime and to boost the data collecting effectivity. Here, a RADMA was introduced as a communication protocol to enhance the received signal power and avoid frequent signal collisions. First, the performance of RADMA in suppressing OP and capturing failure probability was evaluated analytically. Then, the simulation results considering an LPWAN environment elucidated that the derived closed-form expression of OP was valid. Numerical simulation results have validated

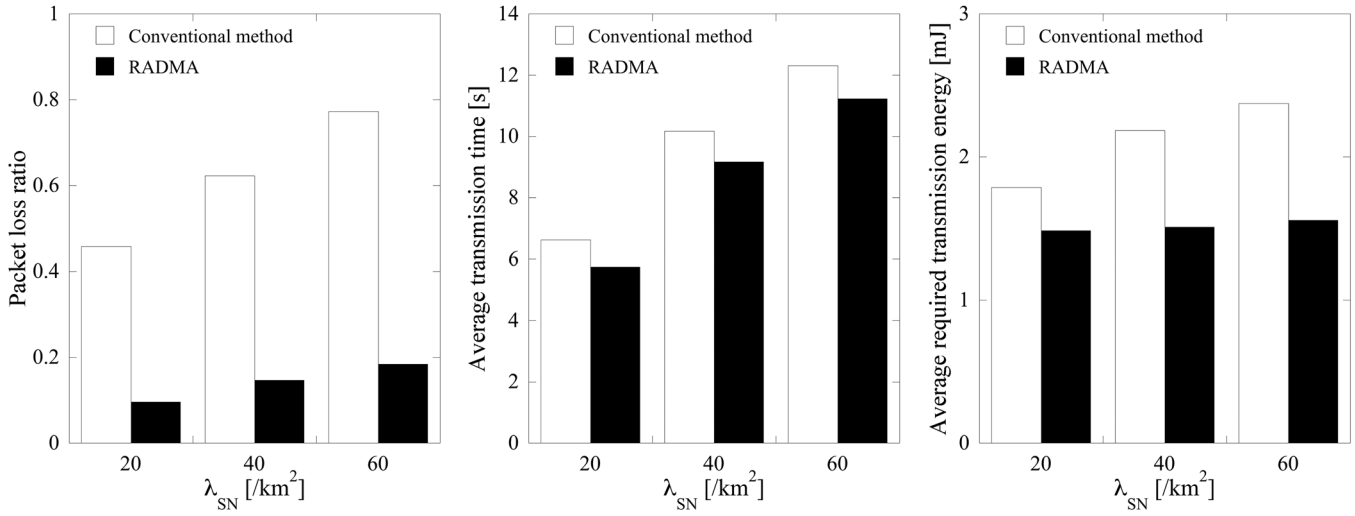

FIGURE 6 Performance comparison of RADMA and conventional method (various intensity of SN λ_{SN})

that RADMA can lower the OP, suppress the PLR 77%, shorten the transmission time 25%, and reduce the required transmission energy 20% when considering an area with L_{AREA}=5 [km] and λ_{SN}=20 [/km^2]. To further improve the performance, interferences from other systems sharing the same unlicensed spectrum need to be appropriately analysed and handled. This is left as our future work.

ACKNOWLEDGEMENTS

This work was supported by JSPS KAKENHI Grant Number JP18K04127.

ORCID

Hendrik Lumbantoruan https://orcid.org/0000-0002-0744-5251
Koichi Adachi https://orcid.org/0000-0003-3463-1233

REFERENCES

1. Abbasi, A., et al.: Wireless sensor node platform for in-plant stress monitoring. Sensors 1–4 (2020). https://ieeexplore.ieee.org/document/9278900
2. Jawad, H.M., et al.: Accurate empirical path-loss model based on particle swarm optimization for wireless sensor networks in smart agriculture. IEEE Sens. J. 20(1), 552–561 (2020)
3. Hu, Z., et al.: Application of non-orthogonal multiple access in wireless sensor networks for smart agriculture. IEEE Access 7, 87582–87592 (2019)
4. Gulec, O., et al.: A novel distributed CDS algorithm for extending lifetime of WSNs with solar energy harvester nodes for smart agriculture applications. IEEE Access 8, 58859–58873 (2020)
5. Sansoy, M., et al.: Empowering wireless sensor networks with RF energy harvesting. In: IEEE International Conference on Signal Processing and Integrated Networks (SPIN), pp. 273–277 (2020)
6. Sornin, N., et al.: LoRaWAN Specifications, LoRa Alliance, San Ramon (2015)
7. Shahin, N., et al.: Hybrid slotted-CSMA/CA-TDMA for efficient massive registration of IoT devices. IEEE J. Mag. 6, 18366–18382 (2018)
8. Zhang, Z., et al.: QoS aware transcoding for live streaming in edge-clouds aided HetNets: An enhanced actor-critic approach. IEEE Trans. Veh. Tech. 68, 11295–11308 (2019)
9. Xiao, Z., et al.: Unmanned aerial vehicle base station (UAV-BS) deployment with millimeter-wave beamforming. IEEE Internet Things J. 7(2), 1336–1349 (2020)
10. Chen, M., et al.: Artificial neural networks-based machine learning for wireless networks: A tutorial. IEEE Commun. Surveys Tuts. 21(4), 3039–3071 (2019)
11. Zhang, B., et al.: Learning-based energy-efficient data collection by unmanned vehicles in smart cities. IEEE Trans. Ind. Informat. 14(4), 1666–1676 (2018)
12. Wang, B., et al.: Optimal altitude of UAV-BS for minimum boundary outage probability with imperfect channel state information. In: IEEE International Conference on Communications (ICCC), 607–611 (2019)
13. Chen, J., et al.: Efficient data collection in large-scale UAV-aided wireless sensor networks. IEEE Wireless Commun. Signal Process. 1–5 (2019). https://ieeexplore.ieee.org/document/8927929
14. Liu, S., et al.: Performance analysis of UAVs assisted data collection in wireless sensor network. In: IEEE 87th Vehicular Technology Conference (VTC Spring), pp. 1–5 (2018)
15. Chen, Y., et al.: Optimum placement of UAV as relays. IEEE Commun. Lett. 22(2), 248–251 (2018)
16. Wang, B., et al.: Optimal altitude of UAV-BS for minimum boundary outage probability with imperfect channel state information. In: IEEE International Conference in Communications in China (ICCC), pp. 607–611 (2019)
17. Shabanighazikelayeh, M., Koyuncu, E.: Outage-optimized deployment of UAVs. In: IEEE Personal, Indoor and Mobile Radio Communications (PIMRC), pp. 1–6 (2019)
18. Pham, H.X., et al.: Cooperative and distributed reinforcement learning of drones for field coverage. arXiv:1803.07250v2
19. Chowdhury, M.M.U., et al.: Trajectory optimization in UAV-assisted cellular networks under mission duration constraint. In: IEEE Radio and Wireless Symposium (RWS), pp. 1–4 (2019)
20. Ozturk, M., et al.: Clustering based UAV base station positioning for enhanced network capacity. In: IEEE Advances in the Emerging Computing Technologies (AECT), pp. 1–6 (2020)
21. Ebrahimi, D., et al.: UAV-aided projection-based compressive data gathering in wireless sensor networks. IEEE Internet Things J. 6(2), 1893–1905 (2019)
22. Lumbantoruan, H., Adachi, K.: Array antenna for power saving of sensor nodes in UAV-BS enabled WSN. In: Proceedings of the IEEE

Inyernational Conference on Networking and Computing, pp. 1024–1028 (2019)
23. Han, G., et al.: Design of high gain cosecant beam-forming array antenna. In: IEEE International Conference on Microwave and Millimeter Wave Technology (ICMMT), pp. 1–3 (2018)
24. Lumbantoruan, H., Adachi, K.: OP analysis of sensor nodes served by an ULA equipped UAV-BS. In: IEICE General Conference (2019)
25. Farhad, A., et al.: Interference-aware spreading factor assignment scheme for the massive LoRaWAN network. In: IEEE International Conference on Electronics, Information, and Communication (ICEIC), pp. 1-2 (2019)
26. Marquez, L.E., et al.: On the use of LoRaWAN in smart cities: A study with blocking interference. IEEE Internet Things J. 7(4), 2806–2815 (2020)
27. Badawy, A., et al.: On the performance of quickest detection spectrum sensing: The case of cumulative sum. IEEE Commun. Lett. 24(4), 749–743 (2020)
28. Molisch, A.F.: Wirel Communication, 2nd edition (2011)
29. Phantom 4 Pro Specs. https://www.dji.com/phantom-4-pro/info (2021). Accessed 6 Mar 2021
30. Al-Hourani, A., et al.: Modeling air-toground path loss for low altitude platforms in urban environments. In: Proceedings of the IEEE Global Communication Conference (GLOBECOM), p. 2898–2904 (2014)
31. Chryssomallis, M.: Smart antennas. IEEE Antennas Propag. Mag. 42(3), 129–136 (2000)
32. Sahoo, P., Riedel, T.: Mean Value Theorems and Functional Equations, World Scientific, Singapore (1998)
33. Elshabrawy, T., Robert, J.: Analysis of BER and coverage performance of LoRa modulation under same spreading factor interference. In: Personal, Indoor, and Mobile Radio Communication (PIMRC) (2018)
34. LoRa Alliance, LoRaWAN 1.1 specification. https://lora-alliance.org/sites/default/files/2018-04/lorawantm_specification_-v1.1.pdf (2020). Accessed 13 July 2020.
35. Georgiou, O., Raza, U.: Low power wide area network analysis: Can LORA scale? IEEE Commun. Lett. 6, 162–165 (2017)
36. Croce, D., et al.: Impact of lora imperfect orthogonality: Analysis of link-level performance. IEEE Commun. Lett. 22, 4 (2018)
37. Waret, A., et al.: LoRa throughput analysis with imperfect spreading factor orthogonality. IEEE Commun. Lett. 8, 2 (2019)
38. FAA, Summary of small unmanned aircraft rule. Available https://www.faa.gov/uas/media/Part_107_Summary.pdf. Accessed 28 Jul 2020
39. Rached, N.B., et al.: A unified moment-based approach for the evaluation of the outage probability with noise and interference. IEEE Trans. Wirel. Commun. 16(2), 1012–1023 (2017)
40. Gradshteyn, I.S., Ryzhik, I.M.: Table of Integrals, Series, and Products 7th ed. Elsevier, Amsterdam (2007)
41. Chung, K.L.: A Course in Probability Theory, 2nd ed. Academic Press, New York (1974)
42. Andras, S., et al.: The generalized marcum Q-function: An orthogonal polynomial approach. Acta Univ. Sapientiae Math. 3(1), 60–76 (2011)
43. Dodd, F., Peele, R.: Some counting problems involving the multinomial expansion. Math Mag. 64(2), 115–122 (1991)
44. Arfken, G.B., Weber, H.J.: Mathematical Methods for Physicists, 6th Edition (2005)
45. Deaño, A., et al.: Strong and ratio asymptotics for Laguerre polynomials revisited. J. Math. Anal. Appl. 403(2), 477–486 (2013)

How to cite this article: Lumbantoruan H, Adachi K. Array antenna equipped UAV-BS for efficient low power WSN and its theoretical analysis. IET Commun. 2021;1–14. https://doi.org/10.1049/cmu2.12238

APPENDIX A

Proof of Lemma 1

Let the CDF of S_k be expressed as [39]

$$F_{S_k}(s_k) = \sum_{n=0}^{\infty} \frac{e^{-K_k} L_n^{(0)}(K_k)(1+K_k)^{n+1}}{(1+n)!\overline{\Omega}_k^{n+1}} s_k^{n+1}, \tag{A1}$$

where n is the order of truncation index, $L_n^{(\alpha)}(\cdot)$ is the generalized Laguerre polynomials of degree n and order α [42]. Let $f(\cdot)$ denote the PDF of $\{S_k\}_{k=0}^{K}$, then $P_{\text{out}}(\gamma_{\text{th}})$ in (21) can be written as

$$P_{\text{out}}(\gamma_{\text{th}}) = P\left(\frac{S_0}{\sigma^2} < \gamma_{\text{th}}\right) \tag{A2}$$

$$= P\left(S_0 < \gamma_{\text{th}}\sigma^2\right) \tag{A3}$$

$$= \int_0^{\gamma_{\text{th}}\sigma^2} f_{S_0}(s_0) ds_0$$

$$= F_{S_0}\left(\gamma_{\text{th}}\sigma^2\right)$$

$$= \sum_{n=0}^{\infty} \frac{e^{-K_0} L_n^{(0)}(K_0)(1+K_0)^{n+1}}{(1+n)!\overline{\Omega}_0^{n+1}} \left(\gamma_{\text{th}}\sigma^2\right)^{n+1}. \tag{A4}$$

Proof of Lemma 2

Let S_0 is considered to be independent from RVs $(S_1, S_2, \ldots, S_I)$. By inserting the CDF of S_k in (A1) into (25), probability $P_{\text{fail}}(\beta_{\text{th}})$ of being failed to be captured can be derived as follows

$$P_{\text{fail}}(\beta_{\text{th}})$$

$$= P(\beta_0 < \beta_{\text{th}}) = P\left(\frac{S_0}{\sum_{i=1}^{I} S_i} < \beta_{\text{th}}\right) \tag{A5}$$

$$= P\left(S_0 < \beta_{\text{th}}\left(\sum_{i=1}^{I} S_i\right)\right) \tag{A6}$$

$$= \int_0^{\infty} \ldots \int_0^{\infty} \int_0^{\beta_{\text{th}}\sum_{i=1}^{I} S_i} f_{S_0}(s_0) ds_0$$

$$f_{S_1}(s_1) \ldots f_{S_I}(s_I) ds_1 \ldots ds_I \tag{A7}$$

$$= \int_0^{\infty} \ldots \int_0^{\infty} F_{S_0}\left(\beta_{\text{th}}\left(\sum_{i=1}^{I} S_i\right)\right)$$

$$f_{S_1}(s_1) \ldots f_{S_I}(s_I) ds_0 ds_1 \ldots ds_I \tag{A8}$$

$$= \int_0^{\infty} \ldots \int_0^{\infty} \sum_{n=0}^{\infty} \frac{e^{-K_0} L_n^{(0)}(K_0)(1+K_0)^{n+1}}{(1+n)!\overline{\Omega}_0^{n+1}} \beta_{\text{th}}^{n+1}$$

$$\times \left(\sum_{i=1}^{I} S_i \right)^{n+1} f_{S_1}(s_1) \dots f_{S_I}(s_I) ds_1 \dots ds_I \tag{A9}$$

$$= \sum_{n=0}^{\infty} \frac{e^{-K_0} L_n^{(0)}(K_0)(1+K_0)^{n+1}}{(1+n)! \overline{\Omega_0}^{n+1}} \beta_{\text{th}}^{n+1} \times \mathbb{E}\left[\left(\sum_{i=1}^{I} S_i \right)^{n+1} \right] \tag{A10}$$

where $\mathbb{E}[\cdot]$ is the expectation value taken with respect to the random vector $(S_1, S_2, \dots, S_I)$. By applying multinomial theorem [43] to (A10), where

$$(S_1 + \cdots + S_I)^n = \sum_{i_1 + \cdots + i_I = n} \binom{n}{i_1, \dots, i_I} \prod_{j=1}^{I} S_i^{i_j}, \tag{A11}$$

we have

$$P_{\text{fail}}(\beta_{\text{th}}) = \sum_{n=0}^{\infty} \frac{e^{-K_0} L_n^{(0)}(K_0)(1+K_0)^{n+1}}{(1+n)! \overline{\Omega_0}^{n+1}} \beta_{\text{th}}^{n+1} \times \mathbb{E}\left[\sum_{i_1 + \cdots + i_I = n+1} \binom{n+1}{i_1, \dots, i_I} \prod_{j=1}^{I} S_i^{i_j} \right]. \tag{A12}$$

Finally, the closed form of $P_{\text{fail}}(\beta_{\text{th}})$ can be expressed as

$$P_{\text{fail}}(\beta_{\text{th}}) = \sum_{n=0}^{\infty} \frac{e^{-K_0} L_n^{(0)}(K_0)(1+K_0)^{n+1}}{(1+n)! \overline{\Omega_0}^{n+1}} \beta_{\text{th}}^{n+1} \times \sum_{i_1 + \cdots + i_I = n+1} \binom{n+1}{i_1, \dots, i_I} \prod_{j=1}^{I} \mathbb{E}[S_i^{i_j}]. \tag{A13}$$

Proof of Theorem 1

By applying the moments of sums of random variables [41] to (A10), where

$$\mathbb{E}\left(\sum_{k=1}^{K} S_k \right)^n \le K^{n-1} \sum_{k=1}^{K} \mathbb{E}(S_k^n), \text{ for } n > 1, \tag{A14}$$

we have

$$P_{\text{fail}}(\beta_{\text{th}}) = \sum_{n=0}^{\infty} \frac{e^{-K_0} L_n^{(0)}(K_0)(1+K_0)^{n+1}}{(1+n)! \overline{\Omega_0}^{n+1}} \beta_{\text{th}}^{n+1} \times \mathbb{E}\left[\left(\sum_{i=1}^{I} S_i \right)^{n+1} \right]$$

$$\le \sum_{n=0}^{\infty} \frac{e^{-K_0} L_n^{(0)}(K_0)}{(1+n)!} \left(\frac{\beta_{\text{th}}(1+K_0)}{\overline{\Omega_0}} \right)^{n+1} \times I^n \left(\sum_{i=1}^{I} \mathbb{E}[S_i^{n+1}] \right). \tag{A15}$$

By using inequality $L_n^{(0)}(x) \le e^{x/2}$ [42], we have

$$P_{\text{fail}}(\beta_{\text{th}}) \le \sum_{n=0}^{\infty} \frac{e^{-K_0/2}}{(1+n)!} \left(\frac{\beta_{\text{th}}(1+K_0)}{\overline{\Omega_0}} \right)^{n+1} \times I^n \left(\sum_{i=1}^{I} \mathbb{E}[S_i^{n+1}] \right) \tag{A16}$$

$$= \sum_{i=1}^{I} \sum_{n=0}^{\infty} \frac{e^{-K_0/2}}{(1+n)!} \left(\frac{\beta_{\text{th}}(1+K_0)}{\overline{\Omega_0}} \right)^{n+1} I^n \mathbb{E}[S_i^{n+1}] = \sum_{i=1}^{I} \sum_{n=0}^{\infty} g_{n,i}. \tag{A17}$$

Inserting the moment corresponding to the Rician model into $g_{n,i}$ yields

$$g_{n,i} = \frac{e^{-K_0/2}}{(1+n)!} \left(\frac{\beta_{\text{th}}(1+K_0)}{\overline{\Omega_0}} \right)^{n+1} I^n \mathbb{E}[S_i^{n+1}] = \frac{e^{-K_0/2}}{(1+n)!} \left(\frac{\beta_{\text{th}}(1+K_0)}{\overline{\Omega_0}} \right)^{n+1} I^n \times \frac{\Gamma(n+2)}{(1+K_i)^{n+1}} {}_1F_1(-(n+1), 1; K_i) \overline{\Omega_i}^{n+1}. \tag{A18}$$

The Kummer confluent hypergeometric function is related to the Laguerre polynomials of degree n and order zero $L_n^0(\cdot)$ as follows [40]:

$${}_1F_1(-n, 1; -x) = L_n^0(-x). \tag{A19}$$

By substituting (A19) into (A18), we have

$$g_{n,i} = \frac{e^{-K_0/2}}{(1+n)!} \left(\frac{\beta_{\text{th}}(1+K_0)}{\overline{\Omega_0}} \right)^{n+1} I^n \times \left(\frac{\overline{\Omega_i}}{1+K_i} \right)^{n+1} \Gamma(n+2) L_{n+1}^0(-K_i). \tag{A20}$$

An asymptotic expression of Gamma function is given as [40]:

$$\Gamma(n+a) \sim_{n \to +\infty} n^a \Gamma(n). \tag{A21}$$

By substituting (A21) into (A20), we have

$$g_{n,k} \sim \frac{\mathrm{e}^{-K_0/2}}{(1+n)!}\left(\frac{\beta_{\mathrm{th}}(1+K_0)\overline{\Omega_i}}{\overline{\Omega_0}(1+K_i)}\right)^{n+1} I^n \times n^2\Gamma(n)L_{n+1}^0(-K_i). \tag{A22}$$

Since for $x > 0$, an asymptotic expression of $L_n^0(-x)$ is given as [45]

$$L_n^0(-x) \sim_{n\to+\infty} \frac{1}{2\sqrt{\pi}} e^{-x/2}(nx)^{-1/4} e^{2\sqrt{nx}}, \tag{A23}$$

by inserting (A23) into (A22), we have

$$g_{n,i} \sim \frac{\mathrm{e}^{-K_0/2}}{(1+n)!}\left(\frac{\beta_{\mathrm{th}}(1+K_0)\overline{\Omega_i}}{\overline{\Omega_0}(1+K_i)}\right)^{n+1} I^n \times n^2\Gamma(n)\frac{1}{2\sqrt{\pi}} e^{-K_i/2}((n+1)K_i)^{-1/4} e^{2\sqrt{(n+1)K_i}}. \tag{A24}$$

Now, the D'Alembert test of convergence [44] is employed to get the convergence radius where a series $\sum_{n=0}^{\infty} u_n$ is convergent if

$$\lim_{n\to\infty} \frac{u_{n+1}}{u_n} < 1. \tag{A25}$$

For $g_{n,i}$ given in (A24), we have

$$\lim_{n\to\infty} \frac{g_{n+1,i}}{g_{n,i}} = \lim_{n\to\infty} \frac{1}{(n+2)} \frac{(n+1)^2}{n} e^{2\sqrt{(n+2)K_i}-2\sqrt{(n+1)K_i}} \times \left(\frac{\beta_{\mathrm{th}}(1+K_0)\overline{\Omega_i}}{\overline{\Omega_0}(1+K_i)}\right) I = \left(\frac{\beta_{\mathrm{th}}(1+K_0)\overline{\Omega_i}}{\overline{\Omega_0}(1+K_i)}\right) I < 1.$$

Thus, the convergence radius of power series $\sum_{n=0}^{\infty} g_{n,k}$ is given by

$$\beta_{\mathrm{th}} < \frac{\overline{\Omega_0}(1+K_i)}{(1+K_0)\overline{\Omega_i} I}, \forall i. \tag{A26}$$